Ultra-wide detuning planar Bragg grating fabrication technique based on direct UV grating writing with electro-optic phase modulation

C. Sima,* J. C. Gates, H. L. Rogers, P.L. Mennea, C. Holmes, M. N. Zervas, and P. G. R. Smith

Optoelectronics Research Centre, University of Southampton, Southampton, SO17 1BJ, UK
Chaotan.Sima@soton.ac.uk

Abstract: A direct UV grating writing technique based on phase-controlled interferometry is proposed and demonstrated in a silica-on-silicon platform, with a wider wavelength detuning range than any previously reported UV writing technology. Electro-optic phase modulation of one beam in the interferometer is used to manipulate the fringe pattern and thus control the parameters of the Bragg gratings and waveguides. Various grating structures with refractive index apodization, phase shifts and index contrasts of up to 0.8×10^{-3}have been demonstrated. The method offers significant time/energy efficiency as well as simplified optical layout and fabrication process. We have shown Bragg gratings can be made from 1200nm to 1900nm exclusively under software control and the maximum peak grating reflectivity only decreases by 3dBover a 250 nm (~32THz) bandwidth.

OCIS codes: (230.1480) Bragg reflectors; (130.0130) Integrated optics; (050.2770) Gratings; (120.3180) Interferometry; (120.5060) Phase modulation; (220.1230) Apodization.

References and links

1. T. Erdogan, "Fiber grating spectra," J. Lightwave Technol. **15**(8), 1277–1294 (1997).
2. K. Okamoto, *Fundamentals of Optical Waveguides*(Academic, 2006).
3. T. Storgaard-Larsen, S. Bouwstra, and O. Leistiko, "Opto-mechanical accelerometer based on strain sensing by a Bragg grating in a planar waveguide,"Sens. Actuator A. **52**(1–3), 25–32 (1996).
4. J. Hübner, S. G. Kjaer, M. Dyngaard, Y. Shen, C. L. Thomsen, S. Balslev, C. Jensen, D. Zauner, and T. Feuchter, "Planar Er- and Yb-doped amplifiers and lasers," Appl. Phys. (Berl.) **73**(5–6), 435–438 (2001).
5. M. Svalgaard, C. V. Poulsen, A. Bjarklev, and O. Poulsen, "Direct UV writing of buried singlemode channel waveguides in Ge-doped silica films," Electron. Lett. **30**(17), 1401–1403 (1994).
6. G. D. Emmerson, S. P. Watts, C. B. Gawith, V. Albanis, M. Ibsen, R. B. Williams, and P. G. R. Smith, "Fabrication of directly UV-written channel waveguides with simultaneously defined integral Bragg gratings," Electron. Lett. **38**(24), 1531–1532 (2002).
7. G.D. Emmerson, C.B. Gawith, R. B. Williams, and P.G.R. Smith, "Ultra-wide detuning through direct grating writing of planar Bragg structures," OSA Topical meeting On Bragg Gratings, Photosensitivity and Poling, OSA Tech. Digest Series, 181–183 (2003).
8. I. Petermann, B. Sahlgren, S. Helmfrid, A. T. Friberg, and P. Y. Fonjallaz, "Fabrication of advanced fiber Bragg gratings by use of sequential writing with a continuous-wave ultraviolet laser source," Appl. Opt. **41**(6), 1051–1056 (2002).
9. Y. Liu, J. J. Pan, C. Gu, F. Zhou, and L. Dong, "Novel fiber Bragg grating fabrication method with high-precision phase control," Opt. Eng. **43**(8), 1916–1922 (2004).
10. M. Gagné, L. Bojor, R. Maciejko, and R. Kashyap, "Novel custom fiber Bragg grating fabrication technique based on push-pull phase shifting interferometry," Opt. Express **16**(26), 21550–21557 (2008).
11. K. M. Chung, L. Dong, C. Lu, and H. Y. Tam, "Novel fiber Bragg grating fabrication system for long gratings with independent apodization and with local phase and wavelength control," Opt. Express **19**(13), 12664–12672 (2011).
12. D. Stepanov and S. Surve, " Fabrication of 1D and 2D grating structures," in *Optical Fiber Communication Conference, 2006 and the 2006 National Fiber Optic Engineers Conference*, Technical Digest (CD) (Optical Society of America, 2006), paper OFF7.

#189861 - $15.00 USD Received 2 May 2013; revised 12 Jun 2013; accepted 13 Jun 2013; published 24 Jun 2013

13. D. Stepanov and M. Sceats, "Method and apparatusforwriting gratingstructures using controlled phase delay between beams," Uni. of Sydney, U.S. Patent Application 12,356,854,(2009).
14. C. Sima, J. C. Gates, H. L. Rogers, P. L. Mennea, C. Holmes, M. N. Zervas, and P. G. R. Smith, "Phase controlled integrated interferometric single-sideband filter based on planar Bragg gratings implementing photonic Hilbert transform," Opt. Lett. **38**(5), 727–729 (2013).
15. C. Sima, J. C. Gates, B. D. Snow, H. L. Rogers, M. N. Zervas, and P. G. R. Smith, "Simple planar Bragg grating devices for photonic Hilbert transformer," in *proceedings of J. Phys.: Conf. Ser.***276**012089(Institute of Physics publishing, 2011).
16. H. Storøy, H. E. Engan, B. Sahlgren, and R. Stubbe, "Position weighting of fiber Bragg gratings for bandpass filtering," Opt. Lett. **22**(11), 784–786 (1997).
17. M. J. Cole, W. H. Loh, R. I. Laming, M. N. Zervas, and S. Barcelos, "Moving fibre/phase mask-scanning beam technique for enhanced flexibility in producing fibre gratings with uniform phase mask," Electron. Lett. **31**(17), 1488–1490 (1995).

1. Introduction

Planar Bragg gratings are desirable integrated waveguide structures, and have a periodic (or aperiodic) perturbation of refractive index along the waveguide length, and so are very similar to fiber Bragg gratings (FBGs) [1]. These devices have been demonstrated for optical communications [2], optical sensors [3] and waveguide lasers and amplifiers [4]. In terms of fabrication, Svalgaard *et al.* [5] pioneered the direct UV writing approach to define buried channel waveguides in Germanium doped silica. Emmerson *et al.* [6, 7] demonstrated an extension of this technique, direct UV grating writing (DGW), which permits simultaneous definition of both channel waveguides and planar Bragg gratings. Anacousto-opticmodulator (AOM) was used to modulate the intensity of two focused laser beams as a function of stage position whilst the stages were translated [6]. Bragg gratings with center wavelengths between 1400nm and 1700nm have been demonstrated [7]. However, there are some limitations in the AOM writing approach, *e.g.* inefficient usage of laser power, and a non-linear relationship in response that complicates the fabrication of synthesized gratings.

UV writing systems for FBG inscription using phase control have been reported in the literature [8–12]. Mechanical methods were used to control the optical phase via piezo actuators, and the angle of incidence with stepper motors [8]. Individual phase masks were used in [9–11], which inevitably limits the flexibility and simplicity of the grating manipulation. In reference [9], an external signal was used to amplitude modulate the writing beam while the fiber was continuously translated. The use of amplitude modulation limits the potential refractive index modulation contrast. In reference [10], a push/pull phase modulation configuration was demonstrated, using two electro-optical phase modulators within the two arms of the interferometer after a phase mask to synchronize the movement of the fringe pattern with the fiber's own velocity. The technique benefits from phase modulation and hence potentially larger grating contrast. However both the techniques described in [9] and [10] are limited by the 100-200μm diameter spot size which constrains the detuning bandwidth; for example in [10] the grating reflection peak uniformity reduces by 3dB within ~2.5nm from the high contrast Bragg wavelength. In an alternative approach [11], the local Bragg wavelength was detuned by moving the phase mask in the direction perpendicular to its surface using a piezoelectric translation stage. However, in this technique the ability to rapidly apodize, chirp or phase shift the grating was limited by the 1 mm spot size of the writing beam. The concept of phase control has also been demonstrated for making grating structures on a photoresist layer using a 413 nm Kr^+ laser [12, 13].

Compared to these schemes, our technique designed for planar waveguides offers improved Bragg grating fabrication features, including ultra-wide Bragg wavelength detuning, flexible design without phase-masks, exclusive software control without any need for optical realignment, and considerable refractive index contrast (Δn_{ac}); resulting in the capability to make gratings of arbitrary profile with compact dimensions.

In this work we demonstrate a phase modulated DGW fabrication technique using an electro-optic modulator (EOM). Phase modulation is applied to one laser beam of the

#189861 - $15.00 USD Received 2 May 2013; revised 12 Jun 2013; accepted 13 Jun 2013; published 24 Jun 2013

focusing interferometer as a photosensitive silica-on-silicon sample is translated at constant speed under the writing spot. Appropriate electronics create a rolling fringe pattern in synchronization with the translation stage; this rolling fringe pattern inscribes a waveguide and grating simultaneously into a photosensitive core layer. An automatic advantage, as a consequence of simultaneous definition of the waveguide and grating, is that zero-dc refractive index changes (Δn_{dc}) are possible [1], in contrast to FBGs where UV exposure always creates an index increase and therefore an unavoidable dc-refractive index change. Since there is neither laser power reduction nor writing speed variation, the method offers at least four times faster writing speeds than the previous AOM based system with grating refractive index modulation (Δn_{ac}) of up to 0.8×10^{-3}achieved [6]. Furthermore, the linear relation between the control signal and modulation depth together with the unaltered uniform effective index greatly simplifies synthesized grating design. By applying apodization to the grating design we can achieve tailored grating responses such as sidelobe suppressed Gaussian gratings and flat-top reflectors. In this work we demonstrate that Bragg gratings can be written from 1200nm to 1900nm in a single step exclusively under software control without any optical alignment changes. Furthermore, the use of small spots allows for grating reflectivity that has only 3dB peak reflection reduction cross the 1400nm to 1650nm range (32THz FWHM). This linear apodization response and ultra-wide detuning capability allows arbitrary planar Bragg gratings to be made with the benefits of integrated chip format, direct thermal tuning, UV phase trimming, and good fiber compatibility, which can also be used alongside conventional etched silica-on-silicon processes.

2. Experimental setup

A schematic of the phase control DGW setup is shown in Fig. 1(a). This DGW method involves focusing two crossed laser beams (λ = 244nm) into the photosensitive core of a planar sample with a spot 6 μm in diameter, illustrated in Fig. 1(b). Phase modulation is applied to one arm of the interferometer via the EOM, this controls the relative position of the interference fringe pattern. Constant translation of the sample and modulation of the fringe pattern position defines the channel waveguide and simultaneously allows creation of the grating structures. The photosensitive platform used in this work is a three-layer silica-on-silicon composite, containing a thermal oxide lower cladding, a photosensitive core and an upper cladding, fabricated using flame hydrolysis deposition (FHD) and hydrogen loaded before use. The core typically has a thickness 5–7μm, ensuring vertical single mode operation, and is doped with germanium for photosensitivity. This platform has been shown to offer waveguide losses below 0.04dB/cm in the telecom C-band (1530–1565 nm).

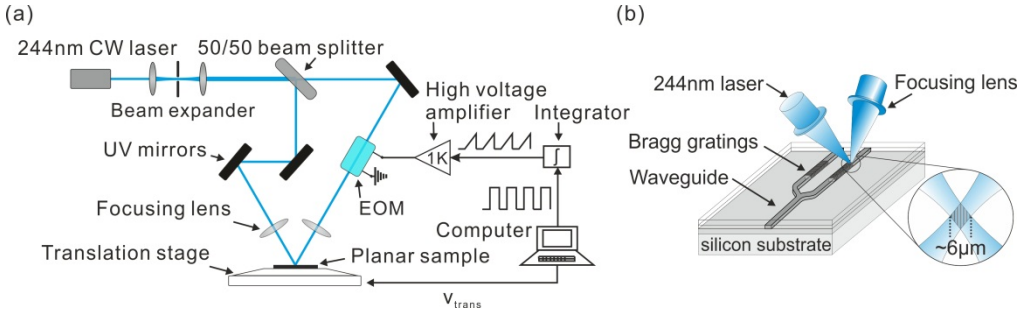

Fig. 1. (a) The experimental setup of the phase modulated direct UV grating writing technique; (b) a 3D illustration of the focused writing spot in the silica-on-silicon sample.

A frequency doubled argon-ion laser (Lexel 95-SHG) produces a100 m WCW output at 244nm, which overlaps the UV absorption bands of the photosensitive core in the germanium doped silica-on-silicon sample. An air-bearing stage system (Aerotech ABL 9000) translates the sample underneath the beams with positional accuracy of 10 nm. UV writing fluence, or

#189861 - $15.00 USD Received 2 May 2013; revised 12 Jun 2013; accepted 13 Jun 2013; published 24 Jun 2013

spot energy density of12kJ/cm^2, allows a writing speed of4 mm/min. Grating parameters, *e.g.* Bragg wavelength, apodization profile and phase shifts are controlled by G-code, a standard computer numerical control software language. The control system generates a rectangular waveform that is fed into an electronic integrator, producing the sawtooth signal in Fig. 2. This signal is then used to drive the EOM via a high voltage amplifier (Trek 610E).Due to inductive traces and capacitive loads, negative over shoot was observed during the rapid high voltage operation, and was alleviated by adding a high voltage diode and resistance to the load.

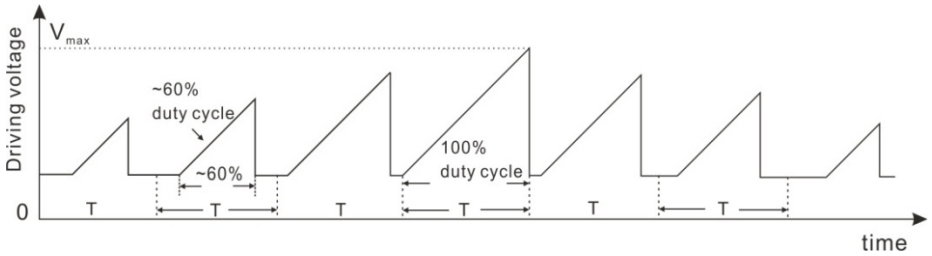

Fig. 2. Schematic of the sawtooth waveform to drive the EOM for fabricating apodized gratings. T denotes the time interval for one grating period.

Figure 2 illustrates the sawtooth signal that is applied so that the fringes follow the sample translation over one grating period. The duty cycle determines the local modulation contrast (Δn_{ac}) of the grating, with 100% duty cycle providing the strongest refractive index change. At the end of the each voltage ramp the fringes jump back to the original drive voltage position. During this brief transition the sample is exposed, giving a slight index increase. The use of a high slew rate amplifier minimizes this unwanted effect. Each new period of the sawtooth signal results in a new sub-exposure of the sample, corresponding to the new sub-grating. In the case of apodized gratings, the sawtooth peak height, and hence the proportion of time for which the pattern tracks the sample, will change for each period, shrunk to some extent compared to the full period pattern (Fig. 2). The diminished ratio is determined by the value of apodization profile (duty cycle value). In this case, the firing position (average voltage point) should remain the same in each period; otherwise the grating period will have avariation that leads to unwanted grating chirp. Hence the sawtooth center needs to be allocated at equal intervals to maintain a constant grating pitch.

Potassium di-hydrogen phosphate (KDP) was used as the EOM crystal, in a longitudinal configuration, which was kept in dry conditions within a sealed housing. With an EOM capacitance of 32pF, the high voltage amplifier allows a sufficient slew rate. The insertion loss of the EOM was 14% (0.75 dB). The optical phase of the laser beam through the crystal is controlled by the applied electric field from the high voltage amplifier.

The two crossed laser beams are focused within the core layer of the planar sample which is precisely aligned to the plane of the translation stage. This ensures Δn_{ac} is uniformly achieved over the length of the waveguide. The crossing angle between the beams is 26° to create an interference pattern with ~535nm period for grating operation in the telecom C-band. This angle could be adjusted to create grating periods suitable for the target wavelength [6].

Figure 3 shows the pre-test and calibration of the UV writing setup. We fabricated a series of uniform and Gaussian apodized gratings in a single chip with increased EOM drive voltages. Figure 3(a) illustrates the dependence of maximum ramp voltage on the grating modulation depth Δn_{ac}. The data shows that maximum modulation is observed at ~4kV and corresponds to a relative optical phase shift of 2π of the Michelson interferometer over one spatial period of translation. To ensure the optimal driving voltage of 4kV is achieved at all Bragg wavelengths the ramp rate of the integrator is also adjusted by the control software. In Fig. 3(b), the grating Δn_{ac} behaves linearly with duty cycle below 0.8, which is a critical

#189861 - $15.00 USD Received 2 May 2013; revised 12 Jun 2013; accepted 13 Jun 2013; published 24 Jun 2013

feature when making apodized gratings. The artifact above 0.8 is a result of the restricted slew rate of the high voltage amplifier. Using a high slew rate amplifier would minimize this unwanted effect. In the following data a duty cycle of 0.8 is used as the maximum duty cycle. Using the same technique, Δn_{ac} of up to 1×10^{-3} has been achieved in high photosensitivity samples.

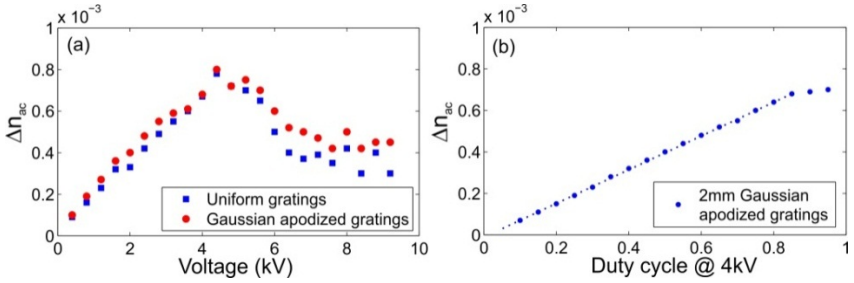

Fig. 3. (a) EOM drive voltage test with uniform gratings (square) and Gaussian apodized gratings (circle); (b) Duty cycle linearity test with 2mm Gaussian apodized gratings.

The UV induced refractive index change that formed the waveguide was ~4×10^{-3}, and as such the maximum experimental visibility is on the order of 25%. In principle there is no inherent limitation on the achievable visibility. In reality the system is limited by the stability and coherence of the source, the alignment of the two UV beams, positional stability of the translation stages and the bandwidth of the phase modulator. One route to increase the contrast would be to improve the bandwidth response of the phase modulator, yielding an estimated additional modulation depth of ~0.2×10^{-3}.

3. Grating responses

In this section, we describe the experimental performance of fabricated planar Bragg gratings. Uniform, phase-shifted and apodized gratings were made using this method.

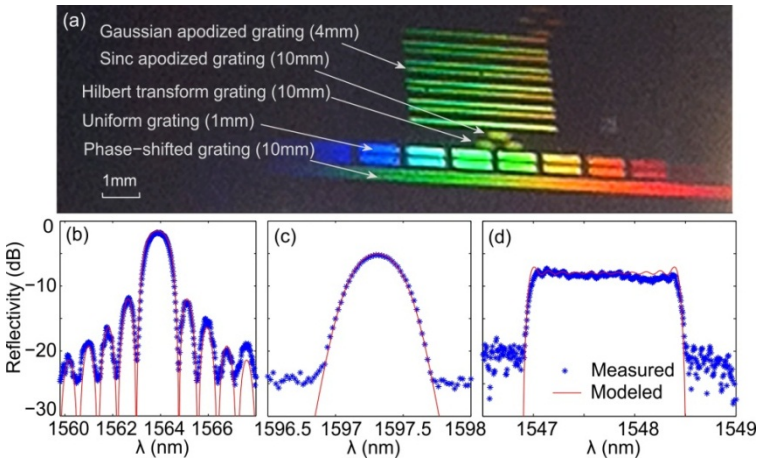

Fig. 4. (a) A white-light source image of grating structures in a sample; (b) The reflectivity spectrum of the uniform grating: experimental data (star dot) and modeled data (red line); (c)Gaussian apodized grating; (d) sinc-apodized grating.

Figure 4(a) shows a photograph of the surface of a planar device containing over20 waveguides with Bragg gratings, including uniform, Gaussian, sinc apodized, Hilbert transformers [14], and phase-shifted gratings [15]. The different colors are due to the incidence-angle dependence of the white light scattered from the inscribed gratings. Figures 4(b)–4(d) exhibit the modeling(red line)and measurement(blue dots) of a 1mm uniform

#189861 - $15.00 USD Received 2 May 2013; revised 12 Jun 2013; accepted 13 Jun 2013; published 24 Jun 2013

grating, 4mm Gaussian apodized grating and a 10mm sinc apodized grating respectively, with the maximum Δn_{ac} of 0.6×10^{-3}. The gratings were characterized using an optical spectrum analyzer (OSA) and a broadband source, the limited source spectral power causes a restricted dynamic range, producing a noise floor at −25dB. In Fig. 4(c), the Gaussian apodized grating has-5dB peak reflectivity and >20dB side lobe suppression, and is likely limited by the characterization limitations. In Fig. 4(d) the sinc-apodized Bragg grating features multiple phase shifts along the grating structure and has a nearly flat-top reflection response with ~200 GHz bandwidth, sharp-cut edges and ~1dB ripple on the top [16]. Such gratings may be employed to produce improved performance in all-optical signal processing filters [14].

4. Ultra-wide grating detuning

As discussed in the introduction, the conventional route for achieving substantial center wavelength detuning *i.e.* greater than tens of nanometers, requires an alternative phase mask to be used or an interferometer to be realigned. However, in a fixed period system, *i.e.* one whereby the angle of the interfering beams is fixed, a detuning process may be applied. The detuning process introduces a differential in the distance between each stepped exposure of an interference pattern and the inherent period of the grating structure [7]; the maximum detuning only depends on the beam spot size, thus small spot sizes allow for larger detuning ranges [17]. The DGW process builds up the grating structure through successive exposure of the small spot interference pattern with a diameter of ~6 μm, with each single snapshot only contributing a fraction of the overall grating exposure at any given point in the grating structure. The additive process and small spot permits fine tuning of the grating structure, allowing an ultra-wide Bragg wavelength detuning range with significant refractive index change. Arbitrary Bragg grating devices can be made for any desired central wavelength via this flexible and reliable method.

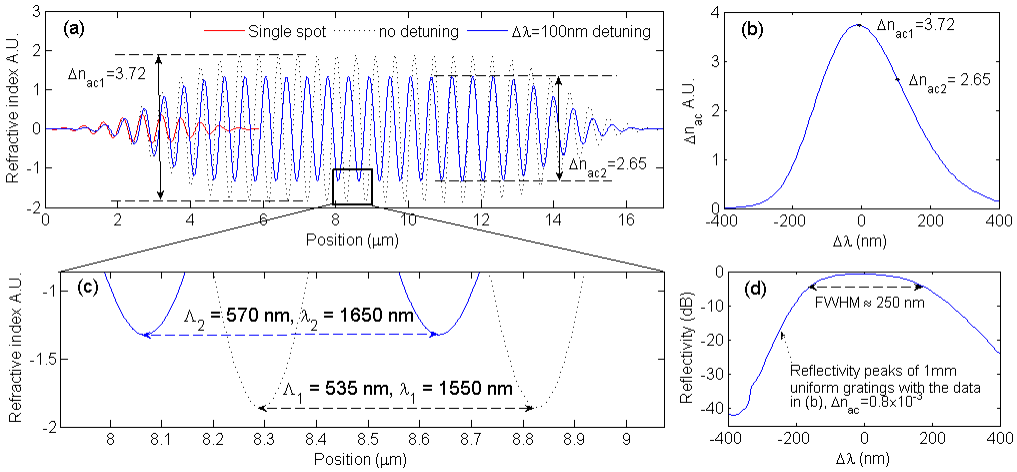

Fig. 5. Modeling: (a) the refractive index pattern along a grating section (note this design is deliberately shortened to illustrate the apodization approach); (b) refractive index change (Δn_{ac}) as a function of wavelength detuning ($\Delta\lambda$) with the phase-controlled method; (c) partial enlarged details in (a) present grating period variation showing wavelength detuning; (d) 1 mm uniform grating reflection peaks variation as a function of $\Delta\lambda$ with 250nm FWHM.

Figure 5 shows the modeling and simulation of the phase controlled DGW process. Figure 5(a) plots refractive index distribution along the grating section for three scenarios; the normalized single interference fringe pattern with a ~6μm diameter Gaussian spot(red line), the zero wavelength detuning pattern (dotted line) and a 100nm wavelength detuning pattern (blue line). The dotted line has an increased refractive index change (Δn_{ac}) due to the additive effect of the overlapping of the single (red line) pattern. The additive effect gives an index of

#189861 - $15.00 USD Received 2 May 2013; revised 12 Jun 2013; accepted 13 Jun 2013; published 24 Jun 2013

modulation 3.72 times that of the single exposure pattern. With detuning (blue line) the index modulation drops to 2.65 time that of the single exposure pattern. Hence the Δn_{ac} reduces by a factor of only 29% with a 100nm change in Bragg wavelength. The DGW technique also offers a zero dc-refractive index change ($\Delta n_{dc} = 0$) with fluence matching [6], and the combination of grating length and refractive index modulation depth Δn_{ac} determines the grating strength. Figure 5(b) shows the maximum refractive index change (Δn_{ac}) as a function of wavelength detuning ($\Delta\lambda$). The highlighted data points (Δn_{ac1}, Δn_{ac2}) correspond to no detuning and 100 nm wavelength detuning scenarios, respectively in Fig. 5(a).

Figure 5(c) shows an enlarged drawing of the square region in Fig. 5(a) and indicates the wavelength detuning ($\Delta\lambda$ = 100nm) and the grating period difference. Figure 5(d) shows the simulation of the maximum reflectivity variation of 1mm long uniform Bragg gratings with $\Delta\lambda$ while the maximum Δn_{ac} is assumed to be 0.8×10^{-3}. The Bragg grating peak reflectivities are predicted to be greater than –20dBover a700nm wavelength range, and it predicts that the –3dB reflectivity degradation in terms of the achievable grating peak wavelength detuning range (the full width at half maximum, FWHM) is ~250nm.

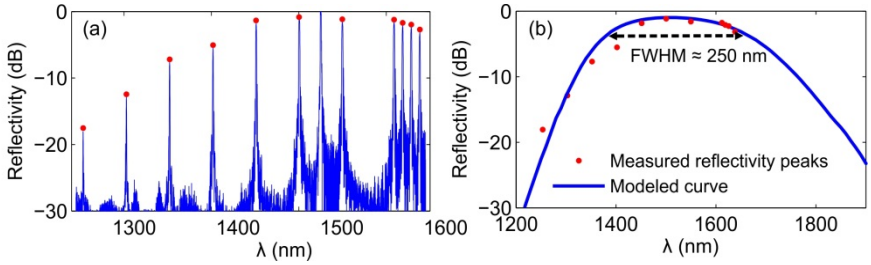

Fig. 6. Experimental demonstration: (a) reflectivity spectrum of the gratings from 1250nm to 1650nm. (b) Grating peak reflectivity (red dot) and modeled curve (solid line).

Using this concept, the process has been demonstrated as a highly flexible fabrication technique capable of producing an ultra-wide range of grating periods in one chip from a single experimental setup. The efficiency of the method is demonstrated in Fig. 6. A series of 1mm long uniform Bragg gratings with a wavelength interval of 50 nm were fabricated in one channel waveguide in a single process; the reflectivity spectrum is illustrated in Fig. 6(a). The reference grating at 1525nm was a 3mm long uniform Bragg grating with a saturated reflection spectrum for characterization calibration. The saturated optical response provides a probe of the optical intensity within the waveguide at a specific spectral position. With this value and knowledge of the spectral response of the source and characterization system, a precise measurement of the reflectivity of other gratings within the waveguide can be determined, removing the principle source of error *i.e.* coupling loss.

Figure 6(b) shows the reflectivity of the gratings (stars) and the modeling curve (blue line) using the data from Fig. 5(d). The grating reflectivity varies slightly around 1400nm which is believed to be due to the hydroxyl ion absorption in the silica material. The experimental results suggest that gratings can be fabricated between 1200nm and 1900nm, and demonstrate that the –3dB bandwidth range (FWHM) is ~250nm (32THz), agreeing with the modeling in Fig. 5(d). This ultra wide detuning range was achieved entirely through software control, without any mechanical perturbation or optical realignment. Bragg gratings with wavelengths over 1650nm were not fabricated due to the limited bandwidth of the characterization setup. In this data the strongest 1mm grating demonstrated ~70% reflectivity and 1.4nm –3dB bandwidth, indicating the grating Δn_{ac} of 0.8×10^{-3}.

This technique can also be used to fabricate longer Bragg gratings in planar or fiber geometries, and the length of such gratings is only limited by the translation distance of the stages, which is currently 300mm. In this case the gratings were purposely kept short to prevent saturation of the optical response. If the gratings were made longer (*e.g.*>2.5mm) then

#189861 - $15.00 USD Received 2 May 2013; revised 12 Jun 2013; accepted 13 Jun 2013; published 24 Jun 2013

the reflectivity variation would saturate and further increase the 250nm reflectivity variation bandwidth shown in Fig. 6(b).

5. Conclusion

The principle and experimental results of an ultra-wide planar Bragg grating fabrication technique using phase-controlled direct UV grating writing have been demonstrated. An electro-optic phase modulator driven by periodic sawtooth signals is placed in one arm of an interferometer setup to manipulate the interference pattern visibility on the material. The grating parameters are software controlled without any perturbation of the writing interferometer. Along with the unique micron-order writing spot, modulation linearity ensures the desired grating apodization profile is achieved. Furthermore, the significant fringe visibility provides the benefits of considerable refractive index change and ultra-wide wavelength detuning range. The flexibility, simplicity, low cost, and stability of this technique make it a powerful and promising tool to fabricate arbitrary planar Bragg gratings.

Acknowledgments

This work was supported by Engineering and Physical Sciences Research Council (EPSRC), UK and China Scholarship Council, China.

#189861 - $15.00 USD Received 2 May 2013; revised 12 Jun 2013; accepted 13 Jun 2013; published 24 Jun 2013